metals

Article

Parameter Optimization for Hydrogen-Induced Fluidized Bed Reduction of Magnetite Iron Ore Fines

Heng Zheng [1,*], Johannes Schenk [1,2,*], Oday Daghagheleh [1] and Bernd Taferner [1]

[1] Department of Metallurgy, Montanuniversitaet Leoben, Franz-Josef-Straβe 18, 8700 Leoben, Austria
[2] K1-MET GmbH, Stahlstraße 14, 4020 Linz, Austria
* Correspondence: heng.zheng@stud.unileoben.ac.at (H.Z.); johannes.schenk@unileoben.ac.at (J.S.)

Abstract: Hydrogen-based direct reduced iron (HyDRI) produced by fluidized bed has great potential for achieving the target of net-zero carbon in steelmaking. However, when magnetite ores were used as feedstock, several process parameters showed influences on its fluidization and reduction behaviors. To confirm the dominant influencing factors and its optimum process condition, the orthogonal experimental method was conducted in the present study. The result shows that the primary and secondary influencing factors are oxidation temperature, oxidation content, MgO addition amount, and gas velocity. The optimum condition is that the magnetite iron ore is deeply oxidized at 800 °C, mixed with 1.5 wt.% of MgO powder, and reduced in the fluidized bed at a gas velocity of 0.45 m/s.

Keywords: hydrogen-based direct reduced iron; fluidized bed; influencing factors; optimum condition

1. Introduction

Steel is the world's most important engineering and construction material [1]. The total production of crude steel in 2020 was 1.95 billion tons, and the top three steel-producing countries were China, India, and Japan, respectively [2]. With the development of developing countries, the steel demand will further increase [3,4]. It is estimated that the global steel demand will grow by more than 60% by 2050 [5]. Iron and steel production is a CO_2 emissions-intensive sector, which was responsible for 2.6 Gt CO_2 emission (about 7% of global anthropogenic CO_2 emissions) in 2019 [6]. The two dominant steelmaking processes are the blast furnace–basic oxygen furnace (BF–BOF) route and the scrap-based electric arc furnace (EAF) route [7,8]. In terms of CO_2 emission, the BF–BOF route emits 1.6–2.2 tons CO_2 per ton of crude steel, which is more than twice the amount CO_2 emission than that of the EAF route (0.6 tons CO_2 per ton of crude steel) [9–11]. To achieve the goal of CO_2 neutrality within the process, the shift from BF–BOF to EAF is a trend for future steelmaking [8]. Due to the limited access to high-quality scrap, it can be partly replaced by direct reduced iron (DRI). The ongoing development of the hydrogen-based direct reduced iron (HyDRI)—EAF route has a high potential for reducing CO_2 emission. When EAF is operated with pure HyDRI, CO_2 emission can be reduced to 25–53 kg per ton of crude steel [12,13]. Therefore, how to produce HyDRI properly and efficiently becomes an interesting topic.

Many commercial processes use shaft furnaces or fluidized bed reactors as iron ore reduction units [14,15]. Fluidized beds usually show better reduction efficiency because of faster mass and heat transfer. An ongoing hydrogen-based-fine-ore reduction process, namely HYFOR, developed by Primetals Technologies, is one of the successful examples [16]. However, if the de-fluidization phenomenon occurs, i.e., the iron ore fines cannot be fluidized by the gas flow, the reduction efficiency would drop dramatically, and process control of the system would become impossible. In a hydrogen-induced fluidized bed, the newly formed metallic iron on the particle surface is sticky and has a high probability

check for updates

Citation: Zheng, H.; Schenk, J.; Daghagheleh, O.; Taferner, B. Parameter Optimization for Hydrogen-Induced Fluidized Bed Reduction of Magnetite Iron Ore Fines. *Metals* **2023**, *13*, 339. https://doi.org/10.3390/met13020339

Academic Editor: Chenguang Bai

Received: 30 December 2022
Revised: 28 January 2023
Accepted: 6 February 2023
Published: 8 February 2023

of forming iron aggregates [17]. To prevent de-fluidization, the particle surface can be modified by coating treatment [18]. One practical method is to mix MgO with the iron ore fines before charging into the fluidized bed reactor. The MgO acts as a physical barrier to reduce the frequency of contact between particles [19]. When the reduction temperature is higher than 900 °C, MgO reacts with Fe_2O_3/FeO and forms Fe_2MgO_4/FeO·MgO on the particle surface, which serves as a chemical barrier [20].

Hydrogen reduction of iron oxide is an endothermic reaction that requires external heat input into the system such as preheating the iron ore. When magnetite iron ore is used, it becomes oxidized in a preheat process. Based on our previous study, the raw magnetite iron ore could not be completely fluidized at the temperature range of 600–800 °C. The generated fresh metallic iron accumulated on the surface of the magnetite particle and an iron shell was formed. While an oxidation treatment of magnetite iron ore improved the fluidization behaviors. The pre-oxidation treatment promoted the formation of a porous structure. The porous structure improved the reducibility and also avoids the formation of iron shell on the particle surface, thus decreasing the de-fluidization tendency. However, additional MgO was still needed when the reduction temperature was higher than 650 °C [21]. It was also found that the oxidation temperature and oxidation content (deeply oxidized or party oxidized) of magnetite influenced the fluidization and reduction behaviors [22]. Higher oxidation temperature shows a better fluidization improvement effect but leads to a lower reduction rate in the later reduction stage. According to kinetic analysis, the diffusion of the iron ions was the rate-limiting step. A lower pre-oxidation temperature could improve the diffusion of the iron ions.

The current study determines the proper operating parameters through an orthogonal experimental method. Furthermore, the dominant factors that influence the fluidization and reduction behaviors of the magnetite iron ore are confirmed. Based on the results, practical guidance can be provided for pilot or industrial trials.

2. Experimental

2.1. Materials

A low raw-grade magnetite iron ore was used as raw material, and the chemical composition is shown in Table 1. The high-purity MgO powder (>99.5 wt.% MgO, size below 44 µm) was used as an anti-sticking additive. The particle size of the raw magnetite ore is in the range of 125–500 µm, which is achieved by mixing 50 wt.% of 125–250 µm and 50 wt.% of 250–500 µm. For the oxidation treatment, 1000 g of the raw magnetite ore was charged into a steel vessel and put into a conventional heat treatment furnace at 800, 900, and 1000 °C for a specific time. To endure a uniform oxidation of magnetite particles within the material layer, the material was stirred manually during the oxidation. Two types of oxidized material, namely partly oxidized material and deeply oxidized material were obtained at each oxidation temperature. It should be noted that oxidation degrees of the deeply oxidized material and partly oxidized material range from 94% to 97% and 50% to 65%, respectively. The oxidation degree was confirmed by the actual weight gain and theoretical weight gain. The theoretical weight gain can be calculated according to FeO content from the chemical analysis of the raw magnetite iron ore. The detailed calculation has been described in detail elsewhere [23].

Table 1. Chemical composition of the raw magnetite iron ore, wt.%.

[1] Fe_{tot}	FeO	SiO_2	Al_2O_3	CaO	MgO	MnO	P
59.50	19.66	7.05	1.13	3.03	2.00	0.17	0.7

[1] Fe_{tot}—Total iron content.

2.2. Apparatus and Methods

The main apparatus in this study, as shown in Figure 1, was a fluidized bed reactor with a 68 mm inner diameter [21,24]. The principle of the experimental apparatus was to measure the weight change and differential pressure drop continuously during the reduction process. The factors affecting the fluidized reduction were selected as oxidation temperature (Factor A), oxidation content (Factor B), MgO addition amount (Factor C), and gas velocity (Factor D). The orthogonal experimental plan was designed using IBM SPSS software (Statistics 26, IBM, Armonk, NY, USA), where three levels of each factor were taken. The reduction temperature and H_2 content were 700 °C and 15.9 Nl/min, respectively, for all the experiments. The gas velocity was controlled by changing N_2 content. A sample of 400 g of the material was taken for each experiment. When the reduction degree reached 95% or the reaction time reached 90 min, the reducing gas was changed to N_2 for cooling. The detailed experimental programs are given in Tables 2 and 3.

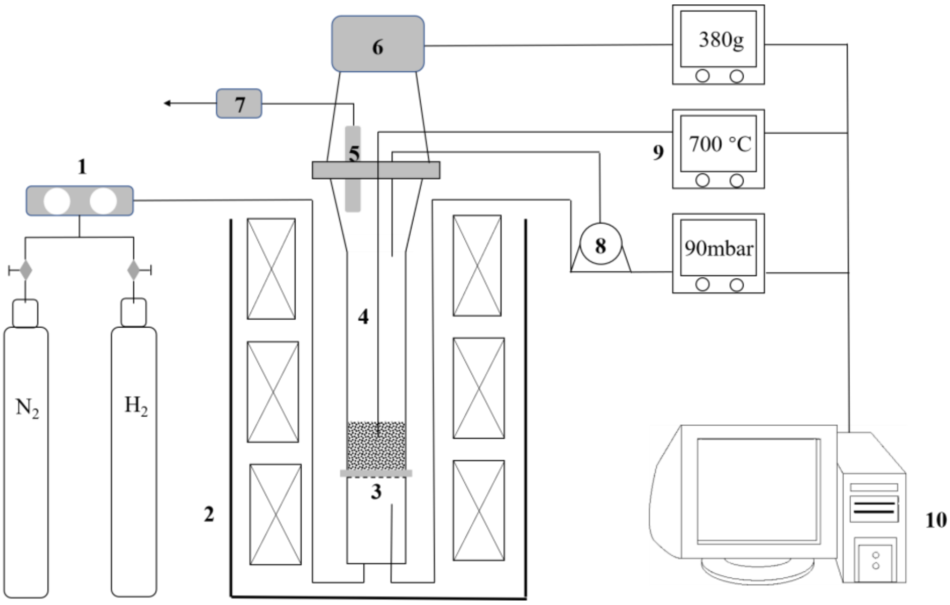

Figure 1. Schematic layout of laboratory fluidized bed reactor [21]: (1) gas system; (2) three-stage electrical furnace; (3) gas distributor; (4) fluidized bed reactor; (5) dust filter; (6) scale; (7) pressure regulator; (8) differential pressure monitor; (9) temperature control; and (10) computer system unit.

Table 2. Orthogonal experimental factors and levels.

Factor	A Oxidation Temperature, °C			B Oxidation Content			C MgO Amount, wt.%			D Gas Velocity, m/s		
Level	A_1 800	A_2 900	A_3 1000	B_1 Raw	B_2 Partly	B_3 Deeply	C_1 0.5	C_2 1.0	C_3 1.5	D_1 0.35	D_2 0.40	D_3 0.45

Table 3. Orthogonal experimental plan.

No.	A	B	C	D
1	A_3	B_2	C_3	D_1
2	A_3	B_3	C_1	D_2
3	A_2	B_1	C_3	D_2
4	A_2	B_3	C_2	D_1
5	A_2	B_2	C_1	D_3
6	A_1	B_3	C_3	D_3
7	A_1	B_1	C_1	D_1
8	A_3	B_1	C_2	D_3
9	A_1	B_2	C_2	D_2

2.3. Definition of Reduction Degree (RD) and Average De-Fluidization Index (Ave.DFI)

The *RD* was defined as the ratio of removed oxygen to the total oxygen bonded to iron, where the removed oxygen was measured by the weight loss. The *RD* can be calculated based on Equations (1)–(3) [21,25,26].

$$RD = \left(1 - \frac{O_{bounded\ \ to\ Fe\ at\ t=ti}}{O_{\ bounded\ to\ Fe\ at\ t=t0}}\right) \times 100\% \tag{1}$$

$$O_{\ bounded\ to\ Fe\ at\ t=ti} = \frac{O_{bounded\ to\ Fe_2O_3} + O_{bounded\ to\ FeO} - \Delta m}{M_O} \tag{2}$$

$$O_{\ bounded\ to\ Fe\ at\ t=t0} = 1.5 \times \frac{m_0 \times Fe_{tot}}{M_{Fe}} \tag{3}$$

where $O_{\ bounded\ to\ Fe\ at\ t=t0}$ and $O_{bounded\ to\ Fe\ at\ t=ti}$ represent the amounts of oxygen that are bounded to iron at the start and during the reduction, Δm and m_0 are the weight loss due to the loss of oxygen and the mass of input material, and M_O and M_{Fe} are the constant molar masses for oxygen and iron.

A de-fluidization index (*DFI*) was introduced previously, as expressed by Equations (4) and (5) [22]. The *DFI* was a real-time value, which represented the portion of material that was not fluidized. For an easier comparison among the experiments in this study, an *Ave.DFI* was defined as shown in Equation (6). The differential pressure data were collected every two seconds. Dividing the total *DFI* by the amount of data gives *Ave.DFI*.

$$DFI = \frac{\Delta p_{calculated-bed} - \Delta p_{measured-bed}}{\Delta p_{calculated-bed} - \Delta p_{Fixed-bed}} \tag{4}$$

$$\Delta p_{calculated-bed} = \frac{m_t \times g}{Reactor\ area} \tag{5}$$

$$Ave.DFI = \frac{\sum DFI}{N_{DFI}} \tag{6}$$

where $\Delta p_{Fixed-bed}$ is the differential pressure drop when the material is in a fixed bed state. $\Delta p_{Fixed-bed}$ is 2 mbar in this work; m_t is the mass of the remaining material in the fluidized bed during the reduction. N_{DFI} is the amount of DFI data.

3. Results and Discussions

3.1. Orthogonal Experiment Analysis

The goal of a fluidized bed reduction is to obtain a high reduction rate at a stable fluidization state. Therefore, the time to reach *RD* = 90% ($t_{90\%}$) and the *Ave.DFI* were chosen as indicators for the optimization of reduction parameters. The result is shown in Table 4**.** Considering the fluctuation of the collected differential pressure data, it can be considered as a completely fluidized bed when the *Ave.DFI* is smaller than 5% [22]. Experiment No.2 shows the lowest *Ave.DFI*, and experiment No.6 shows the smallest $t_{90\%}$. The orthogonal experiment analysis is conducted to confirm the dominant factors that influence the fluidization and reduction behaviors and to figure out the optimum condition. The results are shown In Tables 5 and 6**.** This analysis method is also conducted by Zhang et al. [27] and Xu et al. [28] to determine the optimum fluidized conditions during the reduction of hematite using a CO and CO-H_2 mixture.

The K_i is the sum of the experiment result (see Table 4) for the corresponding level number I as given in Table 3; k_i equals K_i divided by *n*, where *n* is the number occurrences of each level and *n* = 3; R = max{k_i} − min{k_i}. The experimental factor with the highest R-value represents the most dominant influencing factor. The experimental level with the smallest k_i value indicates the optimum choice in the corresponding experimental factor. Therefore, regarding reduction efficiency, i.e., $t_{90\%}$, the primary and secondary influencing factors are oxidation temperature, oxidation content, MgO addition amount, and gas velocity. The optimum condition should be $A_1B_2C_3D_3$: the magnetite iron ore is partly oxidized at 800 °C, mixed with 1.5 wt.% of MgO, and reduced in the fluidized bed at a gas velocity of 0.45 m/s. Regarding the fluidization behaviors, i.e., *Ave.DFI*, the primary and secondary influencing factors are gas velocity, oxidation temperature, MgO addition amount, and oxidation content. The optimum condition should be $D_2A_3C_3B_2$: the magnetite iron ore is partly oxidized at 1000 °C, mixed with 1.5 wt.% of MgO, and reduced in the fluidized bed at a gas velocity of 0.4 m/s. From the orthogonal experimental result given in Table 4, fluidization is not a significant concern under experimental conditions. Experiment No.6 shows the fastest reduction rate. Only experiments No. 4, 5, and 7 are partly de-fluidized. The following discussions mainly concentrate on the reduction rate.

Table 4. The orthogonal experimental result.

No.	$t_{90\%}$**, min**	***Ave.DFI*, %**
1	50.80	2.32
2	70.92	1.73
3	56.64	2.89
4	47.73	16.81
5	49.86	16.95
6	38.62	4.23
7	56.92	18.52
8	66.24	4.56
9	46.95	2.80

Table 5. The orthogonal experimental analysis regarding $t_{90\%}$.

Factor	**A**	**B**	**C**	**D**
K_1	142.49	179.80	177.70	155.45
K_2	154.23	147.61	160.92	174.51
K_3	187.96	157.27	146.06	154.72
k_1	47.50	59.93	59.23	51.82
k_2	51.41	49.20	53.64	58.17
k_3	62.65	52.42	48.69	51.57
R	15.16	10.73	10.55	6.60
Primary and secondary factors			ABCD	
Optimization scheme			$A_1B_2C_3D_3$	

Table 6. The orthogonal experimental analysis regarding *Ave.DFI*.

Factor	**A**	**B**	**C**	**D**
K_1	25.55	25.97	37.20	37.65
K_2	36.65	22.07	24.17	7.42
K_3	8.61	22.77	9.44	25.74
k_1	8.52	8.66	12.40	12.55
k_2	12.22	7.36	8.06	2.47
k_3	2.87	7.59	3.15	8.58
R	9.35	1.30	9.25	10.08
Primary and secondary factors			DACB	
Optimization scheme			$D_2A_3C_3B_2$	

If the condition $A_1B_2C_3D_3$ shows the lowest $t_{90\%}$ with an acceptable *Ave.DFI* (<5.0%), it can be confirmed as the optimum condition. Thereafter, experiment No.10 is carried out using the condition $A_1B_2C_3D_3$. The $t_{90\%}$ and *Ave.DFI* of No.10 are 42.1 min and 2.4%, respectively. The reduction and de-fluidization curves are shown in Figure 2. Experiment No.10 shows a good reduction rate, but still, less than that of experiment No.6. The fluidization behaviors of No.10 and No.6 are similar. Thus, it can be concluded that the experiment. No.6 is the optimum condition instead of No.10.

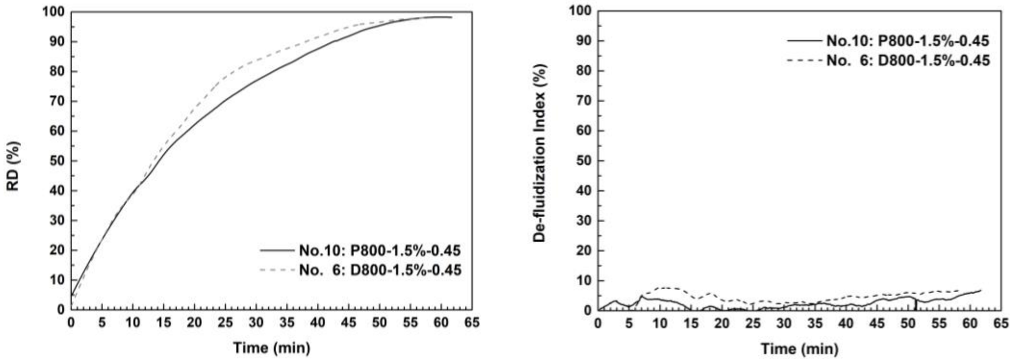

(**a**) (**b**)

Figure 2. The fluidized reduction results of experiments No.6 and No.10: (**a**) reduction curve; (**b**) de-fluidization curve. P800-1.5%-0.45 represents that the magnetite iron ore was partly oxidized at 800 °C, mixed with 1.5 wt.% of MgO and reduced in the fluidized bed at a gas velocity of 0.45 m/s; D800-1.5%-0.45 represents that the magnetite iron ore was deeply oxidized at 800 °C, mixed with 1.5 wt.% of MgO and being reduced in the fluidized bed at a gas velocity of 0.45 m/s.

3.2. The Reduction Curve Analysis

To further understand the orthogonal experimental result, a detailed reduction curve analysis is required. As discussed in Section 3.1, the oxidation temperature and oxidation content are the first two dominant influencing factors. Hence, Figure 3 shows the comparison reduction curve between the samples with different oxidation treatments, where the MgO amount and gas velocity are varied. In Figure 3a, it is shown that the deeply oxidized materials with a higher oxidation temperature give a lower reduction rate. The gaps between the reduction curves are bigger, especially when the reduction degree reaches 80%. As for the raw magnetite sample, the reduction curve presents a different shape, where the reduction rate is not restricted significantly in the later reduction stage. The partly oxidized materials show the same trend that a higher oxidation temperature gives a lower reduction rate (see Figure 3b), whereas the later reduction stages are improved compared with the deeply oxidized materials. This phenomenon is more obvious in the sample oxidized at 1000 °C, as shown in Figure 3c. The samples oxidized at 800 °C are an exception, as it is shown in Figure 2a that the deeply oxidized sample still shows a higher reduction rate than the partly oxidized sample even after reaching the target reduction degree i.e., >90%. For the raw magnetite sample, comparing tests No.8 and No.7, (see Figure 4), it is interesting to note that the test with a higher MgO addition amount and a higher velocity shows a lower reduction rate. It gives a hint that when using magnetite iron ore as raw material, a critical velocity must be determined. It is not that the higher the gas velocity, the faster the reduction rate.

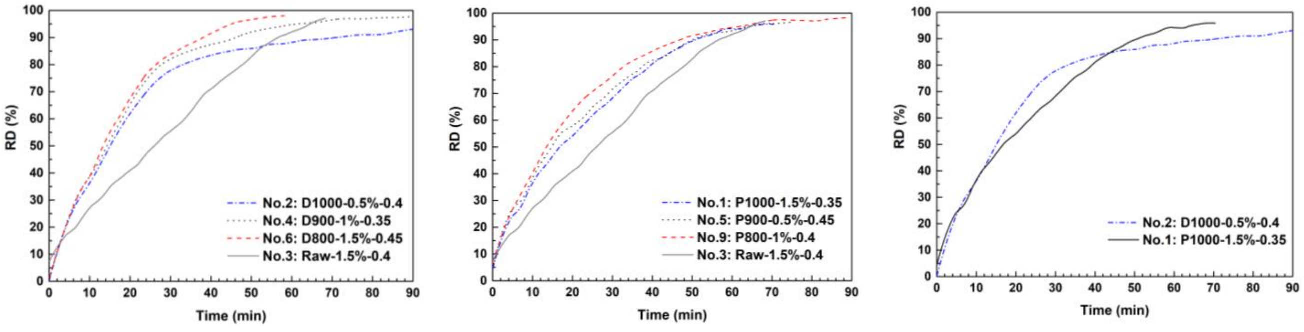

(**a**) (**b**) (c)

Figure 3. The reduction curves of the samples with different oxidation treatments: (**a**) deeply oxidized at different temperatures; (**b**) partly oxidized at different temperatures; (**c**) oxidized at 1000 °C.

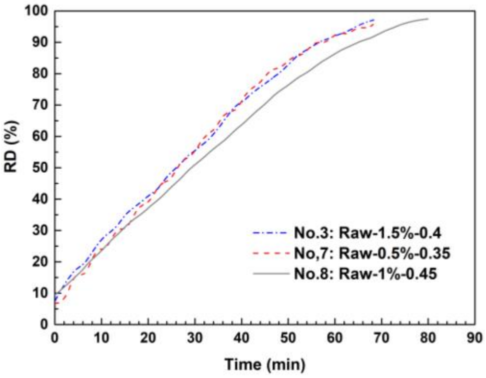

Figure 4. The reduction curves of raw magnetite samples.

3.3. Structural Analysis

To figure out the reason for the reduction behaviors, the morphology of the reduced samples was analyzed via an optical microscope. The reduced particles of the raw magnetite sample are shown in Figure 5. According to Hayes et al. [29,30], the iron morphology obtained by reducing magnetite is mainly controlled by the reduction mechanism. Wolfinger et al. [31] share a similar opinion and found that, for magnetite iron ore ultra-fines, when the reduction is conducted at low temperatures (<675 °C) and controlled by the chemical reaction in the initial reduction stage, a porous iron layer can be formed. However, at higher temperatures (>750 °C), a dense iron layer is formed due to the fast generation of iron and built up in the wüstite. In the present study, the surfaces of the reduced magnetite particles are covered by porous iron layers. From Figure 5a,d, a dense wüstite core is observed, and the porous iron layer is thinner than the other two reduced magnetite samples. It indicates that the reduction of the raw magnetite sample is controlled by the chemical reaction in the initial stage. As the reaction continues, the newly formed iron nuclei accumulate and build a dense iron core within the particles. Iron nuclei accumulate more rapidly at higher gas velocities and form a thinner, porous iron shell, leading to difficulties in gas diffusion within the particles. As shown in Figure 5b,c,e,f, the porous iron shells are much bigger than those in Figure 5a,d. The gas diffuses more easily into the particles, resulting in a higher reduction rate.

As shown in Figure 6a,b,d,e, for the oxidized samples oxidized at 800 °C, the obtained iron morphology is different from that of raw magnetite samples. Instead of porous iron layers, many coarse iron grains are observed on the surface of the particles. From Figure 6c,f, it is seen that, in the sample with oxidation treatment at 1000 °C, the inner part of the reduced particle is porous as well. However, many wüstite islands are observed, indicating a poor reduction behavior. The iron morphology is consistent with our previous study [22]. The oxidation treatment parameters, including oxidation temperature and oxidation content, lead to changes in the reduction kinetic mechanism. The changes in kinetic mechanism are due to the coarse porous wüstite obtained during the reduction of oxidized magnetite [31]. The target of the present study is to confirm the optimum condition for reduction of magnetite ore. The polished section images of reduced samples support the conclusion drawn from the reduction curves, as discussed in Section 3.2.

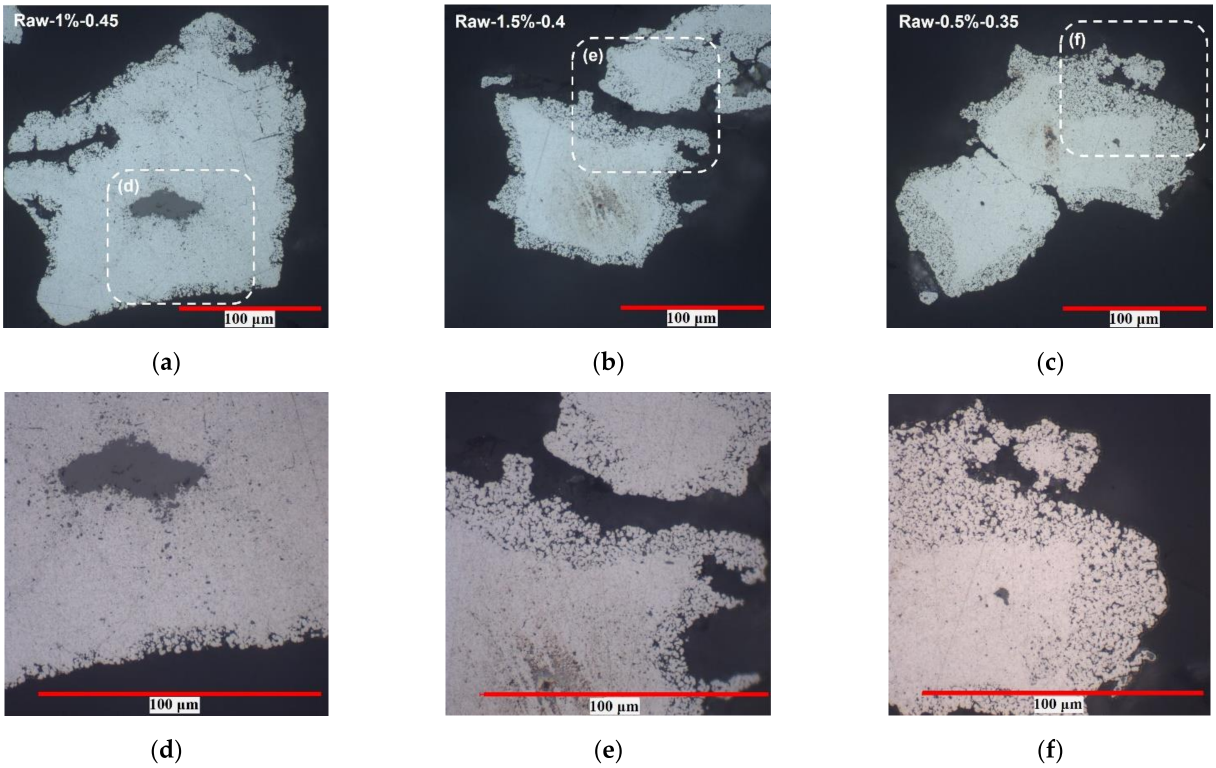

(**a**) (**b**) (**c**)

(**d**) (**e**) (**f**)

Figure 5. The polished section images of reduced iron ores: (**a**,**d**) Experiment No.8; (**b**,**e**) Experiment No.3; (**c**,**f**) Experiment No.7.

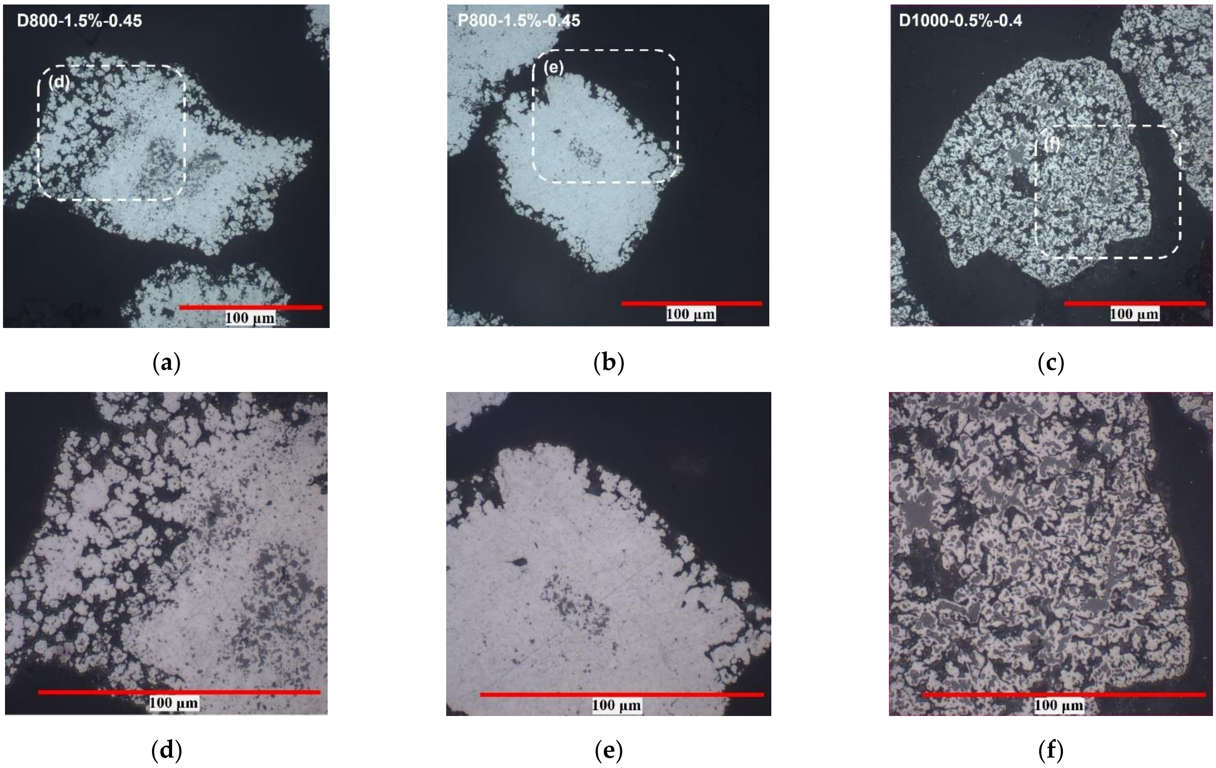

(**a**) (**b**) (**c**)

(**d**) (**e**) (**f**)

Figure 6. The polished section images of reduced iron ores: (**a**,**d**) Experiment No.6; (**b**,**e**) Experiment No.10; (**c**,**f**) Experiment No.2.

4. Conclusions

In conclusion, the optimum condition for hydrogen-induced fluidized bed reduction of magnetite iron ore fines is successfully determined by an orthogonal experimental method. Furthermore, the dominant factors that influence the reduction behaviors of the magnetite iron ore are confirmed. Under the experiment's conditions, the fluidization behavior is not a problem. Regarding reduction efficiency, the primary and secondary influencing factors are oxidation temperature, oxidation content, MgO addition amount, and gas velocity. The optimum condition is that the magnetite iron ore is deeply oxidized at 800 °C, mixed with 1.5 wt.% of MgO, and reduced in the fluidized bed at a gas velocity of 0.45 m/s.

Author Contributions: Conceptualization, H.Z.; methodology, H.Z. and B.T.; investigation, H.Z. and O.D.; writing—original draft preparation, H.Z.; writing—review and editing, J.S., O.D. and B.T.; supervision, J.S.; project administration, J.S.; funding acquisition, J.S. All authors have read and agreed to the published version of the manuscript.

Funding: This research was funded by K1-MET GmbH, metallurgical competence center (funding number FFG No. 869295). The research work was partially financed by Montanuniversitaet Leoben. Heng Zheng greatly acknowledges the financial support from the program of China Scholarship Council (No.201908420284).

Data Availability Statement: Not applicable.

Acknowledgments: All authors greatly acknowledge the funding support of K1-MET GmbH. The research program of the K1-MET competence center is supported by COMET (Competence Center for Excellent Technologies), the Austrian program for competence centers. COMET is funded by the Federal Ministry for Climate Action, Environment, Energy, Mobility, Innovation and Technology, the Federal Ministry for Digital and Economic Affairs, the provinces of Upper Austria, Tyrol and Styria, and the Styrian Business Promotion Agency (SFG).

Conflicts of Interest: The authors declare no conflict of interest.

Nomenclature

Symbol	Description	Unit
HyDRI	Hydrogen-based direct reduced iron	-
BF–BOF	Blast furnace–basic oxygen furnace	-
EAF	Electric arc furnace	-
RD	Reduction degree	%
DFI	De-fluidization index	%
Ave.DFI	Average de-fluidization index	%
$t_{90\%}$	The time to reach the reduction degree of 90%	min

References

1. World Steel Association. About Steel. Available online: https://worldsteel.org/about-steel/about-steel/ (accessed on 19 November 2022).
2. World Steel Association. Total Production of Crude Steel. Available online: https://worldsteel.org/steel-topics/statistics/world-steel-in-figures-2022/ (accessed on 19 November 2022).
3. Bhaskar, A.; Assadi, M.; Nikpey Somehsaraei, H. Decarbonization of the Iron and Steel Industry with Direct Reduction of Iron Ore with Green Hydrogen. *Energies* **2020**, *13*, 758. [CrossRef]
4. Kim, J.; Sovacool, B.K.; Bazilian, M.; Griffiths, S.; Lee, J.; Yang, M.; Lee, J. Decarbonizing the iron and steel industry: A systematic review of sociotechnical systems, technological innovations, and policy options. *Energy Res. Soc. Sci.* **2022**, *89*, 102565. [CrossRef]
5. Rethink. Global Steel Demand to Grow 60% through 2050 Global Steel Demand to Grow 60% through 2050. Available online: https://rethinkresearch.biz/articles/global-steel-demand-to-grow-60-through-2050/ (accessed on 19 November 2022).
6. International Energy Agency. *Iron and Steel Technology Roadmap*; OECD: Paris, France, 2020; p. 37. [CrossRef]
7. He, K.; Wang, L. A review of energy use and energy-efficient technologies for the iron and steel industry. *Renew. Sustain. Energy Rev.* **2017**, *70*, 1022–1039. [CrossRef]
8. Li, Z.; Hanaoka, T. Plant-level mitigation strategies could enable carbon neutrality by 2060 and reduce non-CO_2 emissions in China's iron and steel sector. *One Earth* **2022**, *5*, 932–943. [CrossRef]
9. Patisson, F.; Mirgaux, O. Hydrogen Ironmaking: How It Works. *Metals* **2020**, *10*, 922. [CrossRef]

10. Toktarova, A.; Karlsson, I.; Rootzén, J.; Göransson, L.; Odenberger, M.; Johnsson, F. Pathways for Low-Carbon Transition of the Steel Industry—A Swedish Case Study. *Energies* **2020**, *13*, 3840. [CrossRef]
11. Birat, J.-P. Society, Materials, and the Environment: The Case of Steel. *Metals* **2020**, *10*, 331. [CrossRef]
12. Bellona Foundation. Hydrogen in Steel Production: What Is Happening in Europe—Part Two. Available online: https://bellona.org/news/industrial-pollution/2021-05-hydrogen-in-steel-production-what-is-happening-in-europe-part-two (accessed on 14 November 2021).
13. Vogl, V.; Åhman, M.; Nilsson, L.J. Assessment of hydrogen direct reduction for fossil-free steelmaking. *J. Cleaner Prod.* **2018**, *203*, 736–745. [CrossRef]
14. Schenk, J.L. Recent status of fluidized bed technologies for producing iron input materials for steelmaking. *Particuology* **2011**, *9*, 14–23. [CrossRef]
15. Ma, Y.; Souza Filho, I.R.; Bai, Y.; Schenk, J.; Patisson, F.; Beck, A.; van Bokhoven, J.A.; Willinger, M.G.; Li, K.; Xie, D.; et al. Hierarchical nature of hydrogen-based direct reduction of iron oxides. *Scr. Mater.* **2022**, *213*, 114571. [CrossRef]
16. Daniel, S.; Johann, W.; Bernhard, H.; Norbert, R.; Thomas, W.; Wolfgang, S.; Alexander, F. HYFOR–Hydrogen-based Fine-Ore Reduction. *Mitsubishi Heavy Ind. Tech. Rev.* **2022**, *59*, 1–5. Available online: https://www.mhi.co.jp/technology/review/pdf/e592/e592070.pdf (accessed on 19 November 2022).
17. Guo, L.; Gao, H.; Yu, J.; Zhang, Z.; Guo, Z. Influence of hydrogen concentration on Fe_2O_3 particle reduction in fluidized beds under constant drag force. *Int. J. Miner. Metall. Mater.* **2015**, *22*, 12–20. [CrossRef]
18. Guo, L.; Bao, Q.; Gao, J.; Zhu, Q.; Guo, Z. A Review on Prevention of Sticking during Fluidized Bed Reduction of Fine Iron Ore. *ISIJ Int.* **2020**, *60*, 1–17. [CrossRef]
19. Shao, J.; Guo, Z.; Tang, H. Effect of Coating MgO on Sticking Behavior during Reduction of Iron Ore Concentrate Fines in Fluidized Bed. *Steel Res. Int.* **2013**, *84*, 111–118. [CrossRef]
20. Du, Z.; Zhu, Q.; Yang, Y.; Fan, C.; Pan, F.; Sun, H.; Xie, Z. The Role of MgO Powder in Preventing Defluidization during Fluidized Bed Reduction of Fine Iron Ores with Different Iron Valences. *Steel Res. Int.* **2016**, *87*, 1742–1749. [CrossRef]
21. Zheng, H.; Spreitzer, D.; Wolfinger, T.; Schenk, J.; Xu, R. Effect of Prior Oxidation on the Reduction Behavior of Magnetite-Based Iron Ore During Hydrogen-Induced Fluidized Bed Reduction. *Metall. Mater. Trans. B* **2021**, *52*, 1955–1971. [CrossRef]
22. Zheng, H.; Daghagheleh, O.; Wolfinger, T.; Taferner, B.; Schenk, J.; Xu, R. Fluidization behavior and reduction kinetics of pre-oxidized magnetite-based iron ore in a hydrogen-induced fluidized bed. *Int. J. Miner. Metall. Mater.* **2022**, *29*, 1873–1881. [CrossRef]
23. Zheng, H.; Schenk, J.; Xu, R.; Daghagheleh, O.; Spreitzer, D.; Wolfinger, T.; Yang, D.; Kapelyushin, Y. Surface Morphology and Structural Evolution of Magnetite-Based Iron Ore Fines During the Oxidation. *Metall. Mater. Trans. B* **2022**, *53*, 1644–1660. [CrossRef]
24. Spreitzer, D.; Schenk, J. Fluidization behavior and reducibility of iron ore fines during hydrogen-induced fluidized bed reduction. *Particuology* **2020**, *52*, 36–46. [CrossRef]
25. Skorianz, M.; Mali, H.; Pichler, A.; Plaul, F.; Schenk, J.; Weiss, B. Reduction Behavior and Structural Evolution of Iron Ores in Fluidized Bed Technologies. Part 1: Method for the Determination. *Steel Res. Int.* **2016**, *87*, 633–641. [CrossRef]
26. Pichler, A.; Mali, H.; Plaul, F.; Schenk, J.; Skorianz, M.; Weiss, B. Reduction Behavior and Structural Evolution of Iron Ores in Fluidized Bed Technologies-Part 2: Characterization and Evaluation of Worldwide Traded Fine Iron Ore Brands. *Steel Res. Int.* **2016**, *87*, 642–652. [CrossRef]
27. Zhang, B.; Wang, Z.; Gong, X.; Guo, Z. A comparative study of influence of fluidized conditions on sticking time during reduction of Fe_2O_3 particles with CO. *Powder Technol.* **2012**, *225*, 1–6. [CrossRef]
28. Xu, Q.; Wang, H.; Fu, Y.; Wang, J. Parameters Optimization, Sticking Mechanism and Kinetics Analysis of Fine Iron Ore in Fluidized-Reduction Process. *ISIJ Int.* **2016**, *56*, 1929–1937. [CrossRef]
29. Matthew, S.P.; Cho, T.R.; Hayes, P.C. Mechanisms of porous iron growth on wustite and magnetite during gaseous reduction. *Metall. Mater. Trans. B* **1990**, *21*, 733–741. [CrossRef]
30. Matthew, S.P.; Hayes, P.C. Microstructural changes occurring during the gaseous reduction of magnetite. *Metall. Mater. Trans. B* **1990**, *21*, 153–172. [CrossRef]
31. Wolfinger, T.; Spreitzer, D.; Zheng, H.; Schenk, J. Influence of a Prior Oxidation on the Reduction Behavior of Magnetite Iron Ore Ultra-Fines Using Hydrogen. *Metall. Mater. Trans. B* **2022**, *53*, 14–28. [CrossRef]